Journal of Applied Fluid Mechanics, Vol. 18, No. 4, pp. 1086-1097, 2025.
Available online at www.jafmonline.net, ISSN 1735-3572, EISSN 1735-3645.
https://doi.org/10.47176/jafm.18.4.2899

Effect of Pressure Equalization Groove Structure on Static Characteristics of Aerostatic Bearings

C. Yuanqi[1], X. Yaping[1†], L. Weining[1] and G. Ning[2]

[1] *School of Mechanical Engineering, Jiangsu University of Technology, Wujin, Changzhou, Jiangsu 213016, China*
[2] *Jiangsu JITRI Jingkai High Value Manufacturing Co. Ltd. Kunshan, Suzhou, Jiangsu 215300, China*

†*Corresponding author: xyp@jsut.edu.cn*

ABSTRACT

In order to improve the load capacity and stiffness, the pressure-equalizing groove is introduced into the structure of aerostatic bearing, which can optimize the mechanics characteristics. A Computational Fluid Dynamics (CFD) simulation of bearing with gas-lubricant is developed. The effects of pressure-equalizing groove depth, width, length, number, and supply air pressure on the load capacity, stiffness, and flow rate of orifice-throttle gas bearings are individually analyzed using COMSOL Multiphysics simulation software. The results are then experimentally validated. The results demonstrate that a groove structure designed to equalize pressure can enhance the load-bearing capacity and rigidity of orifice-throttle aerostatic bearings. The static performance of aerostatic bearing increase with the depth, width, number, and supply air pressure of the pressure-equalizing grooves. The peak stiffness of the bearing is significantly enhanced as the depth, width, and supply air pressure of the pressure-equalizing grooves increase. Moreover, the change of grooves number influence the geometric parameter of the air film associated with the maximum stiffness. Different depths, numbers, and supply air pressures of the pressure-equalizing grooves significantly impact the flow rate. In contrast, the variations in width and length have a minor effect. The numerical simulation findings reveal a 71.67% increase in maximum load-bearing capacity and an 81.20% rise in peak stiffness for gas-floating bearings incorporating pressure-equalizing groove structures. Lastly, the congruence between experimental and simulated stiffness curve variations underscores the validity and robustness of the simulation methodology.

Article History

Received June 14, 2024
Revised November 13, 2024
Accepted November 21, 2024
Available online February 4, 2025

Keywords:

Aerostatic Bearings
Pressure-Equalizing Grooves
Static Performance
Finite Element Simulation

1. INTRODUCTION

Compared to traditional bearings, aerostatic bearings offer advantages such as low friction, high precision, no pollution, and low heat generation. These characteristics make them crucial components in the precision and ultra-precision fields, playing significant roles in high-speed spindles, aerospace, lithography machines, wafer inspection, and national defense and military sectors (Liu et al., 2003; Chen et al., 2018; Lu et al., 2020; Gao et al., 2021; Zhang, 2021). However, due to air compressibility, aerostatic bearings are characterized by low load capacity and stiffness, significantly limiting their applications in scenarios requiring high load and stiffness (Belforte et al., 2011; Zhao et al., 2022; Zhang et al., 2023a). Therefore, enhancing aerostatic bearings' load capacity and stiffness remains a key research focus.

As a crucial component for pressure compensation in the aerostatic bearing, the restrictor has a direct impact on the performance of the bearing. Common throttling methods include orifice throttling (Stout & Sweeney 1984), slot throttling (Sharma et al., 1999), porous material throttling (Yoshimoto et al., 2003), equalizing grooves (Du et al., 2012), and equalizing chamber throttling (Kodnyanko et al., 2021). The throttling effect is generated by the compressed gas as it passes through the restrictor, which modifies the pressure distribution of air film, subsequently enhancing the load capacity and rigidity of the aerostatic bearing. The increase of static performance for aerostatic bearing is limited by the throttling method (Chen et al., 2002; Otsu et al., 2011; Yan et al., 2019). Kodnyanko et al. (2021) investigated a double-row radial gas static bearing with longitudinal micro-grooves and output flow regulators. This composite throttling structure can reduce circumferential

air leakage, increasing bearing load capacity and maintaining system stability. Aligning with the Industry 4.0 context, Gou et al. (2021) suggested utilizing multiscale modeling and analytical techniques in the creation and enhancement of aerostatic bearing rails along with their digital counterparts, thereby enhancing the machining quality of ultra-precision machine tools and refining the user experience.

Chen & Chen (2021) developed a multi-field coupling dynamic model of a five-degree-of-freedom aerostatic electric spindle by considering the interaction between the air film, spindle, and motor. The authors used the alternating direction implicit (ADI) and Thomas methods to solve the transient Reynolds equation for the aerostatic and thrust bearings. Moreover, the authors obtained the expected transient pressure distribution of the air film and the spindle's motion trajectory. The results indicated that the impact of spindle tilt on the air film pressure distribution is crucial in determining the restoring force and torque of aerostatic bearings. Zhao et al. (2022) utilized computational fluid dynamics (CFD) techniques to investigate how variations in oil supply pressure, orifice size, and the quantity of orifices influence the static performance of bearings under varying air film thicknesses. The researchers ensured that both the orifice size and the operational air film thickness were maintained within a similar range of values. The results showed that reducing the orifice diameter enhances bearing stiffness. On the other hand, increasing the quantity of orifices improves load capacity but limits stiffness.

Zhang et al. (2023a) conducted a study in which they utilized both single-row and double-row orifice throttling techniques. This innovative approach enabled them to create various designs for equalizing groove structures, specifically linear, extended, and X-shaped configurations. These structures featured rectangular cross-sections and were integrated into the working surface of the rail, showcasing a meticulous engineering adaptation aimed at enhancing functionality. The researchers investigated how various factors influence the load-bearing capacity, rigidity, and air usage of the structure featuring an equalizing groove. The authors established a theoretical foundation for enhancing the static performance of the rail system. Shang et al. (2022) compared the effects of different arrangements and geometric parameters of surface micro-texture structures on lubrication characteristics. The authors reduced the wall's maximum shear force by roughly 15%. They increased the load-carrying capacity (LCC) by approximately 18% by setting partial flow direction textures at the rear end of the expansion wedge. Li et al. (2017) developed a hydrodynamic drag reduction analysis model for functional surfaces with micro-structures on the rail to reduce air resistance during the high-speed motion of aerostatic rails in ultra-precision machine tools. They compared the drag reduction effects of rectangular, V-shaped, U-shaped, and Space-V grooves. The authors found that V-shaped and U-shaped grooves reduce drag, identifying the optimal microstructural parameters for aerostatic rails in ultra-precision machine tools.

Yan & Zhang (2021) conducted an extensive study of the effects of air film thickness, air supply pressure, rotational speed, disturbance amplitude, disturbance frequency, and groove cross-sectional area on the performance of gas static thrust bearings using dynamic mesh technology (DMT) and user-defined function (UDF) combined simulation methods. They concluded that triangular and trapezoidal groove gas static thrust bearings are characterized by superior dynamic stiffness and damping coefficients compared to those with no grooves or rectangular grooves. Zhao et al. (2017) addressed the low stiffness of gas static bearings by developing a gas static thrust bearing with elastic equalizing pressure grooves (EEPG). They obtained the load capacity and stiffness of EEPG static bearings across various air film gap scenarios. The results indicated a 59% increase in stiffness. Wang & Lin (2023) employed finite difference, perturbation, and hybrid techniques to determine the maximum nonlinear pressure distribution in the system to analyze and predict the dynamic characteristics of elastic rotors supported by non-uniform grooved air-bearing systems. The findings can effectively forecast the behavior of non-uniform slot air bearing (NSAB) systems, establishing a theoretical foundation for the design of future NSAB systems and measures to counter instability.

In summary, a single throttling method offers limited improvement in bearing load capacity and stiffness (Chen et al., 2002; Otsu et al., 2011; Yan et al., 2019). For the limitation problem of static performance for aerostatic bearing in engineering application, we present an innovation design of an equalizing groove structure based on the orifice throttling. Compared with the traditional characteristics (rectangular, triangular and trapezoidal grooves (Papadopoulos et al., 2011; Kumar & Sharma, 2019; Zhang et al., 2023b), this new structure generates an optimized throttling effect that promotes a more uniform pressure distribution across the air film in the vicinity of the orifice and groove regions. The study further utilizes COMSOL Multiphysics simulations to systematically model the influence of key design parameters, including groove depth, width, length, quantity, and air supply pressure, on critical performance metrics such as load capacity, stiffness, and volumetric flow rate. The trends in performance parameters are mapped across these variables to guide optimal design decisions. To validate the simulation results, prototype bearings were fabricated, and comparative experiments were conducted with and without the equalizing grooves. The experimental data confirm the reliability and practical applicability of the finite element simulation method, emphasizing the potential of this novel groove structure to enhance the performance of aerostatic bearings in high-precision applications.

2. CFD MODEL AND PARAMETER SETTINGS

2.1 Structure Modeling

Orifice throttling was selected as the basis for the aerostatic bearing design in this study due to its widespread use, mature technology, and ease of fabrication. A new pressure equalization groove structure

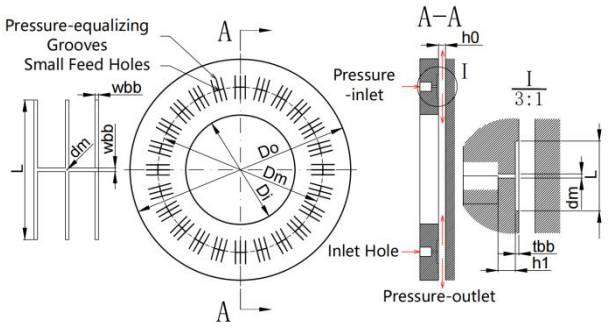

Fig. 1 Schematic diagram of pressure-equalizing grooves aerostatic bearing structure

Table 1 Main construction dimensions of pressure equalization groove

Symbol	Parameters	Value
D_o	Outer diameter (mm)	190
D_i	Inner diameter (mm)	94
D_m	Orifice pitch circle diameter (mm)	142
d_m	Orifice diameter (mm)	0.12
h_1	Orifice length (mm)	0.5
h_0	Air film thickness (mm)	10
tbb	Groove depth (mm)	0.02
wbb	Groove width (mm)	0.5
L	Groove length (mm)	20
N	Number of grooves	6
P	Air pressure (MPa)	0.5

is incorporated to enhance performance. Figure 1 illustrates the design of the pressure equalization grooves, while Table 1 provides a summary of the relevant key parameters. These parameters include air film thickness h_0, outer diameter D_o, inner diameter D_i of the aerostatic bearing, 24 evenly distributed orifices along a pitch circle diameter D_m, orifice diameter d_m = 0.12 mm, orifice height h_1 = 0.5 mm, pressure equalization groove depth *tbb*, width *wbb*, length *L*, number of grooves *N*, and supply pressure *P*.

2.2 Calculation of Static Performance

In Figure 1, the pressure at the aerostatic bearing's air inlet is denoted by *P*. Compressed air flows through the orifice throttling device and the pressure equalization grooves, forming a combined throttling effect before entering the top of the aerostatic bearing. The air quickly fills the entire bearing clearance, forming an air film that generates load capacity and stiffness, thereby supporting the aerostatic bearing (Gao et al., 2015).

The following assumptions are established before calculations to theoretically describe the gas flow model within the aerostatic bearing and calculate the load capacity and stiffness (Chen et al. 2022).

1. The lubricating gas is a Newtonian fluid with constant viscosity.
2. The bearing surface and the table plane are ideally smooth, and the air film thickness h_0 remains constant.
3. The lubricating gas exists as a continuous, single-phase medium.
4. The fully developed gas flow within the air film is an isothermal process, ensuring laminar flow.
5. The pressure and gas density within the air film are constant in the direction of acting force.

The following governing equations for gas flow can be derived based on these assumptions:

The continuity equation, derived from the law of mass conservation:

$$\frac{\partial \rho}{\partial t}+\frac{\partial(\rho u)}{\partial x}+\frac{\partial(\rho v)}{\partial y}+\frac{\partial(\rho w)}{\partial z}=0 \tag{1}$$

where ρ denotes the gas density, while the components of velocity in the *x*, *y*, and *z* directions are indicated by *u*, *v*, and *w*, correspondingly.

The equation of motion, derived from the law of conservation of momentum:

$$\rho\frac{D\vec{V}}{Dt}=\rho\vec{f}-\nabla p+\mu\nabla^2\vec{V}+\frac{\mu}{3}\nabla\left(\mu\nabla\cdot\vec{V}\right) \tag{2}$$

where μ represents dynamic viscosity $\nabla=\frac{\partial}{\partial x}\vec{\imath}+\frac{\partial}{\partial y}\vec{\jmath}+\frac{\partial}{\partial z}\vec{\kappa}$.

The ideal gas law is represented by the equation:

$$\frac{p}{\rho}=gRT \tag{3}$$

where *p* represents the final pressure on the working surface of the aerostatic bearing, *g* is the gravitational acceleration. *R* and *T* are constant and temperature of air.

The simplified Reynolds equation under laminar flow conditions is written to:

$$\frac{\partial}{\partial x}\left(\frac{\rho h_0^3}{\mu}\cdot\frac{\partial p}{\partial x}\right)+\frac{\partial}{\partial y}\left(\frac{\rho h_0^3}{\mu}\cdot\frac{\partial p}{\partial y}\right)=0 \tag{4}$$

where h_0 represents air-film thickness and μ denotes the viscosity of the gas.

The equation for calculating the gas film's load-bearing capacity is:

$$W=\int_s p\,ds \tag{5}$$

where *s* denotes the action area of aerostatic bearing.

The equation for calculating the gas film's stiffness is:

$$K=\frac{W(h+\Delta h)+W(h-\Delta h)}{2\Delta h} \tag{6}$$

where Δh is variation vale of gas film thickness.

2.3 Aerostatic Bearing Mesh Division

The refinement level of the mesh is adjusted to verify the dependency of the numerical solution on mesh discretization by assessing the stability and accuracy of the solution. The optimal number of mesh elements is selected with respect to the computational time. All other conditions are held constant, and only the mesh density of the aerostatic bearing varies. Then, the load-carrying capacity of the equalizing groove should progressively stabilize as the mesh is refined. When the mesh reaches

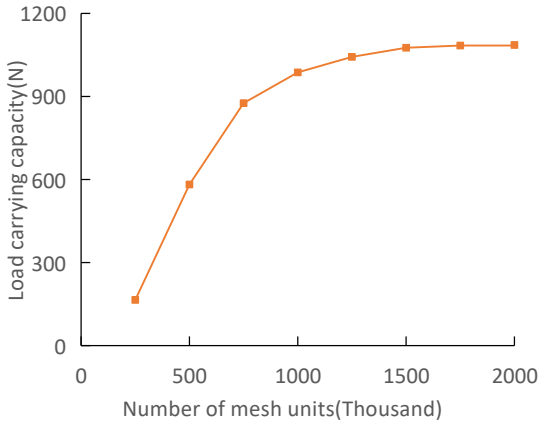

Fig. 2 Mesh independence verification

1,500,000 elements, the variation in load-carrying capacity becomes negligible and stabilizes, indicating that the mesh is adequately refined and further refinement will not significantly enhance the results. Figure 2 illustrates the mesh independence curve.

Given the symmetry in geometric structures, material properties, boundary conditions of the throttling orifice aerostatic bearing, and the symmetry of the load, as well as the load symmetry, a quarter-section air domain model has been chosen to enhance computational efficiency and reduce processing time. The fluid computational domain is divided into the throttling orifice, pressure equalization groove and air-film.

A 3D model of aerostatic bearing can be constructed in COMSOL to enhance mesh quality and computational accuracy. The air-film is utilized to 10 layers, which is built by free triangular meshing with layer sweeping. In order to improve the simulation accuracy, the model in critical regions is refinement, which can represent the influence of structure parameters on the static performance. The interface is used in the junction area of throttling orifice and groove.

The overall mesh count for the aerostatic bearing surpasses 1.5 million, with the precise figure differing according to factors like the depth, width, length, and quantity of the pressure equalization groove. Figure 3 shows the computational fluid dynamics (CFD) model of the pressure equalization groove aerostatic bearing.

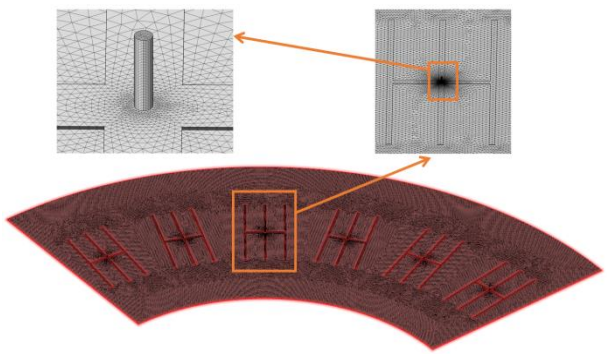

Fig. 3 CFD model of pressure-equalizing grooves aerostatic bearing structure

Table 2 Gas Parameters Setting

Parameters	Value
Temperature/K	293.15
Density/(kg/m^3)	1.204
Dynamic Viscosity/(Pa·s)	1.81×10^{-5}
Molecular Mass/(kg/mol)	28.97×10^{-3}
Specific Heat Capacity/(J/(kg·k))	1.01×10^{3}
Thermal Conductivity/(W/(m·k))	2.42×10^{-2}

Note: Experimental parameters are based on data at a standard atmospheric pressure of 101.325 kPa.

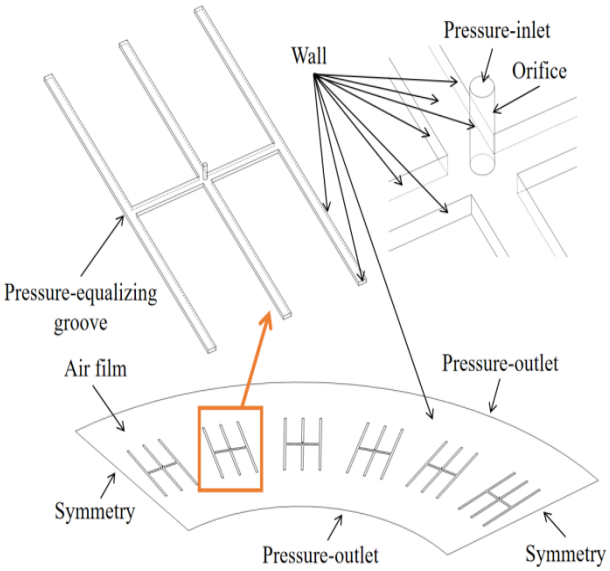

Fig. 4 Schematic diagram of boundary conditions of pressure-equalizing grooves aerostatic bearing structure

2.4 Boundary Condition Settings for Aerostatic Bearings

A laminar flow model is employed to accurately analyze the aerostatic bearing's three-dimensional Computational Fluid Dynamics (CFD) model. The gas within the aerostatic bearing is assumed to be ideal with a constant supply pressure. The convergence criterion is set at 10^{-6}. Gas parameters are detailed in Table 2.

Figure 4 illustrates the boundary conditions for the pressure equalization groove aerostatic bearing. Fluid inlet boundary conditions in COMSOL include velocity inlet, pressure inlet, mass flow inlet, and fully developed flow inlet conditions. This study utilizes pressure inlet and pressure outlet boundary conditions to enhance the convergence of the solution. The throttling orifice inlet is designated as a pressure inlet, with the supply gas pressure set to P. The annular gas film's inner and outer diameters are arranged as pressure outlets, with the external environmental pressure defined at the standard atmospheric level of 101.325 kPa. The left and right lateral surfaces are treated as symmetric boundaries with smooth walls. All other boundaries are specified as no-slip and adiabatic walls.

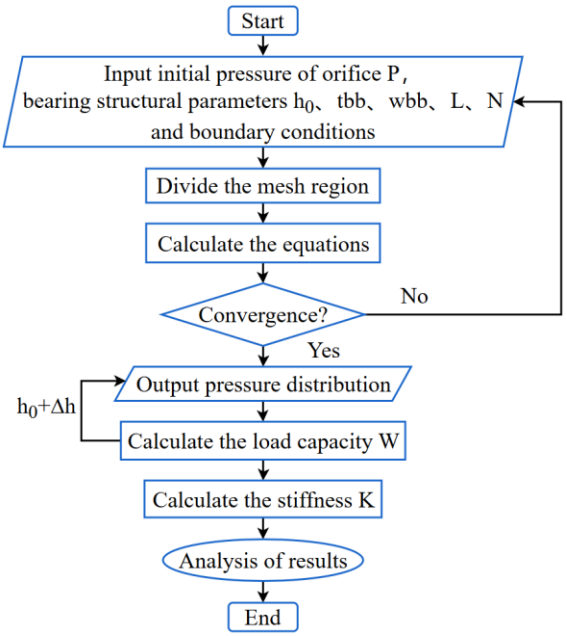

Fig. 5 Calculation process of COMSOL CFD model

3. ANALYSIS OF AEROSTATIC BEARING SIMULATION RESULTS

Simulations were carried out with COMSOL, as discussed earlier, to examine how the structure of the pressure equalization groove affects the static characteristics of aerostatic bearing with throttling orifice. An analysis was performed on aerostatic bearings both with and without pressure equalization grooves. Figure 5 represents the flowchart of the computational process. The primary structural features of the aerostatic bearings used in the simulations are consistent with the previously described specifications. The environmental temperature was 293.15 K, the supply gas pressure was P = 0.5 MPa, while the external atmospheric pressure was adjusted to the standard value of 101.325 kPa.

Pressure distribution contour plots were generated for both types of aerostatic bearings. The simplified 1/4 sector model was visualized as a complete geometric representation, providing greater clarity and intuitiveness. Figure 6 illustrates the pressure distribution contour plot for aerostatic bearings at N = 24, with air-film thickness (h_0=10 μm).

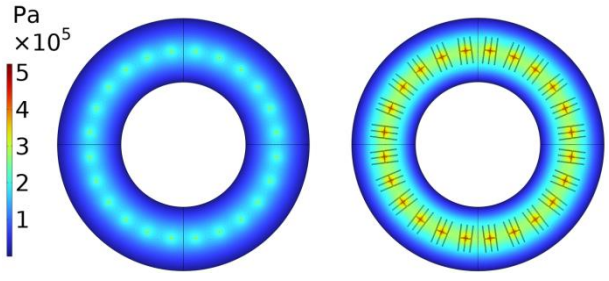

(a) without grooves (b) with grooves

Fig. 6 Pressure distribution cloud map of aerostatic bearings

Fig. 7 Variation in load capacity, stiffness, and flow rate with and without grooves

A comparison of Figs 6(a) and 6(b) reveals that gas enters the orifice from the inlet and passes through the pressure equalization groove to reach the bottom circular gas film. The maximum pressure is observed at the center of the orifice and the groove for pressure equalization. The pressure gradually decreases as the gas diffuses towards the internal and external races of the bearing. The aerostatic bearing with pressure equalization grooves demonstrates a slower pressure drop rate than the bearing without, resulting in a more gradual pressure gradient. Consequently, the pressure value of gas-film is enhanced, especially surrounding the pressure equalization groove. The pressure distribution in the aerostatic bearing with pressure equalization grooves is significantly superior to that in the bearing without such grooves.

Figures 7(a), 7(b), and 7(c) reveal that the maximum load capacity of the structure with pressure equalization

grooves increased by 71.67% compared to the throttling orifice without pressure equalization grooves. In addition, the peak stiffness improved by 81.20%. Thus, the inclusion of pressure equalization groove designs greatly improves the load-bearing capacity and rigidity of the aerostatic bearing with a throttling orifice. However, this improvement increases gas consumption.

Considering that the shaft head is made of metal and is characterized by insufficient surface flatness accuracy, the gas film clearance of the aerostatic bearing is generally designed as 10 μm or higher. Simulations were conducted for various depths *tbb*, widths *wbb*, lengths *L*, numbers *N*, and supply gas pressures *P* of the 1/4 pressure equalization groove aerostatic bearing model to explore the impact of different structural dimensions and parameters of pressure equalization grooves on the lubricant feature of throttling orifice aerostatic bearing. The emulation outcomes are then analyzed and compared.

3.1 Influence of Pressure Equalization Groove Depth

The primary structural dimensions of the aerostatic bearing remain unchanged to examine how the depth of the pressure equalization groove affects the mechanics characteristics of throttling orifice aerostatic bearing. However, other parameters were modified (*wbb* = 0.5 mm, *L* = 20 mm, *N* = 6, *P* = 0.5 MPa). Simulations were conducted to obtain the internal gas's load capacity, stiffness, and volume flow rate for pressure equalization groove depths *tbb* of 0.01 mm, 0.02 mm, 0.03 mm, 0.04 mm, and 0.05 mm. The results indicate that the pressure equalization groove depth significantly affects the mechanics characteristics of aerostatic bearing, as illustrated by the performance curves in Fig. 8.

Figure 8(a) illustrates that as the gas film thickness raises, the load capacity steadily diminishes. However, for a fixed gas film thickness, the load capacity rises with deeper pressure equalization grooves. Figure 8(b) demonstrates that stiffness increases with pressure equalization of groove depth. The stiffness for a pressure equalization groove depth of 0.01 mm is higher than that for 0.02 mm within the gas film thickness range of 9-13 μm. The stiffness peaks within the gas film thickness range of 12-14 μm; beyond 14 μm, the stiffness decreases with the pressure equalization groove depth. Figure 8(c) shows that increasing the pressure equalization groove depth from 0.04 mm to 0.05 mm has a minor effect on the flow rate. However, when the gas film thickness exceeds 14 μm, a deeper pressure equalization groove significantly increases the flow rate.

Adjusting the depth of the pressure equalization groove can enhance the flow characteristics of the gas between the bearings, reduce flow resistance, and improve bearing performance. However, this adjustment also leads to increased gas consumption due to the higher flow rate through the bearing. Therefore, increasing the depth of the pressure equalization groove can boost the load-bearing ability and stiffness of aerostatic bearing with a throttling orifice. However, this improvement comes with a corresponding increase in flow rate.

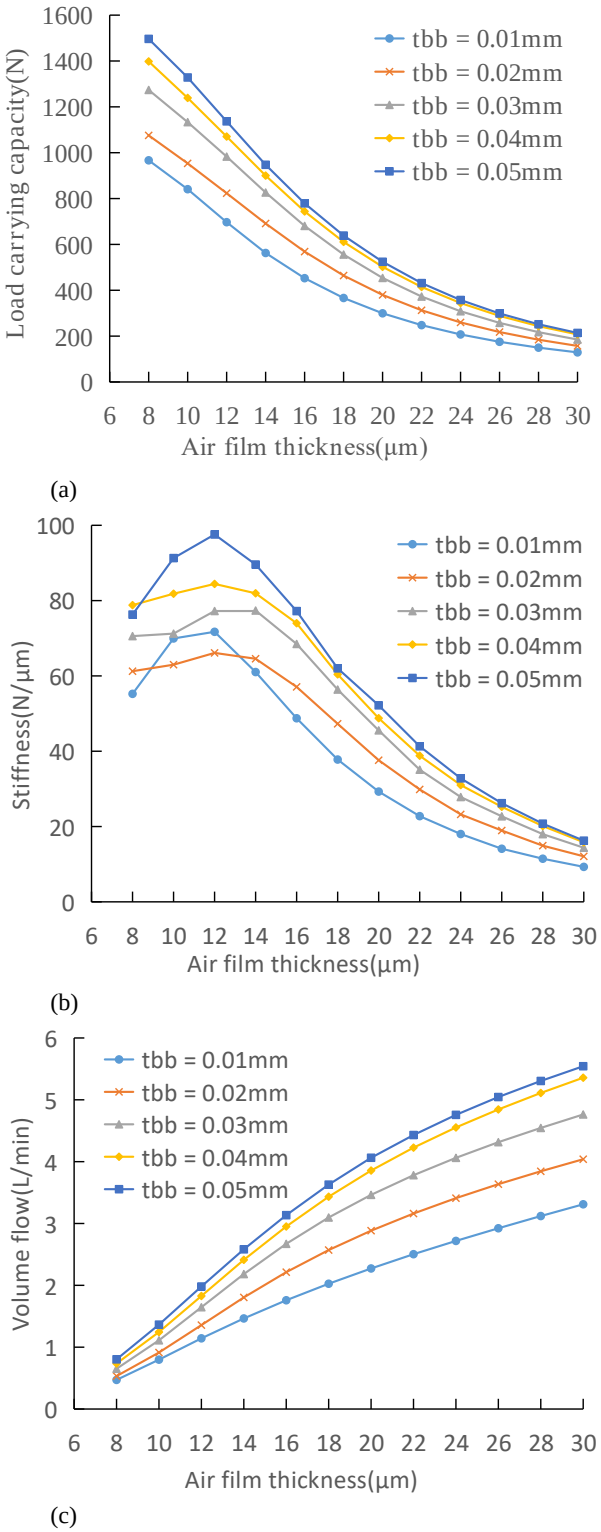

Fig. 8 Variation in load capacity, stiffness, and flow rate with different pressure-equalizing groove depths

3.2 Influence of Pressure Equalization Groove Width

This subsection investigates the effect of pressure equalization groove width on the static characteristic of throttling orifice aerostatic bearing. The structural dimensions of the aerostatic bearing were kept consistent with those described earlier. At the same time, other parameters are modified (*tbb* = 0.02 mm, *L* = 20 mm, *N* = 6, and *P* = 0.5 MPa). Simulations were main conducted

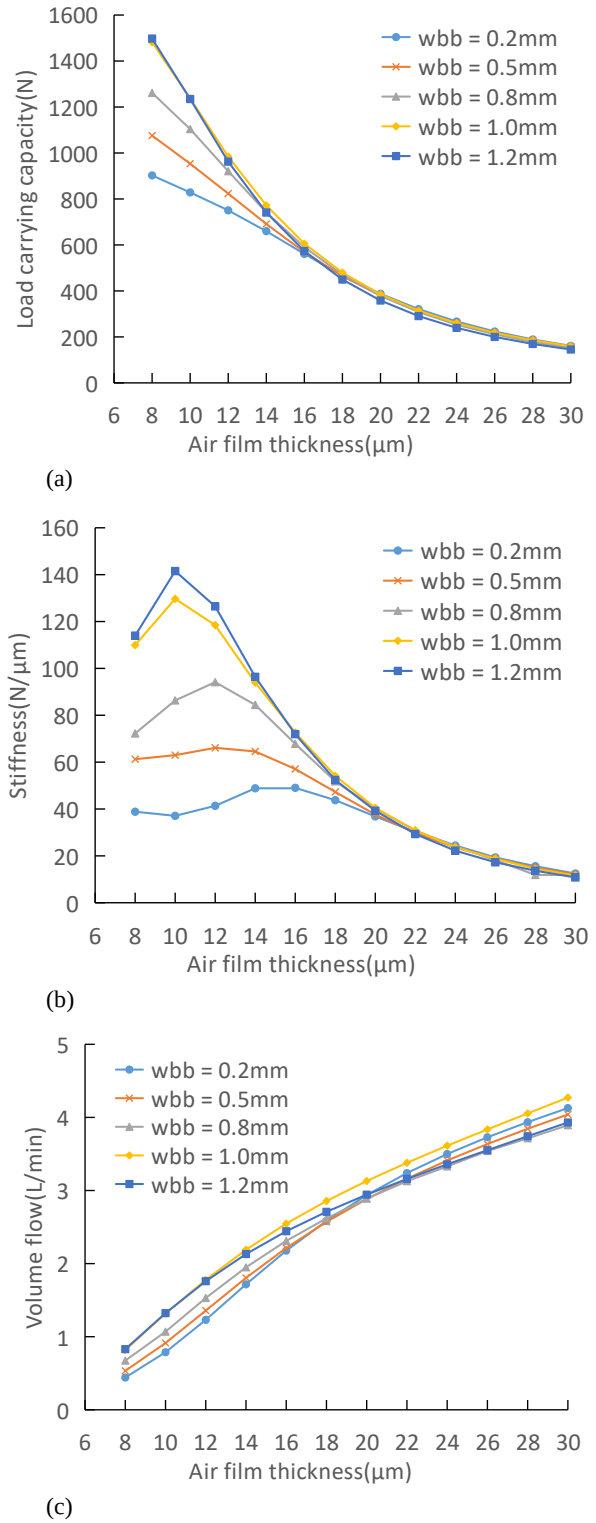

Fig. 9 Variation in load capacity, stiffness, and flow rate with different pressure-equalizing groove widths

to obtain the internal gas's load capacity, stiffness, and volume flow rate for pressure equalization groove widths *wbb* of 0.2 mm, 0.5 mm, 0.8 mm, 1.0 mm, and 1.2 mm. Figure 9 demonstrates how the width of the pressure equalization groove affects the static performance of aerostatic bearing with a throttling orifice.

According to Fig. 9(a), a notable increase in load capacity occurs when the width of pressure equalization groove is expanded from 0.2 mm to 1.0 mm, particularly with a gas film thickness ranging from 8 μm to 12 μm. The load capacity varies slightly within this gas film thickness range. However, no significant change occurs when the width is increased to 1.2 mm. Once the gas-film thickness surpasses 16 μm, the effect of the width of the pressure equalization groove on load capacity becomes practically insignificant.

Figure 9(b) illustrates that increasing the pressure equalization groove width from 0.2 mm to 1.0 mm within a gas film thickness range of 8 μm to 20 μm significantly enhances stiffness. The increase in stiffness is relatively small when the width is increased to 1.2 mm. Additionally, increasing the width has almost no effect on stiffness when the gas film thickness exceeds 20 μm. The peak stiffness shifts to the left as the width increases.

According to Fig. 9(c), when the the gas-film thickness exceeds 12 μm, the flow rate for a width of 1.0 mm is higher than that for a width of 1.2 mm. As the the gas-film thickness grows to 18 μm, the flow rate for a 0.8 mm width is less than the flow rate observed for a 0.5 mm width. In contrast, the flow rate for a width of 0.2 mm is higher than that for a width of 0.5 mm.

A wider pressure equalization groove can distribute the load more evenly and reduce the local deformation of the gas film. The results of the simulation suggest that widening the pressure equalization groove enhances the load capacity and stiffness of aerostatic bearing, significantly affecting the flow rate.

3.3 Influence of Pressure Equalization Groove Length

The effect of pressure equalization groove length on the mechanics characteristics of throttling orifice aerostatic bearing is next studied. The primary structural dimensions of the aerostatic bearing stay aligned with those previously outlined. At the same time, other parameters are modified (*tbb* = 0.02 mm, *wbb* = 0.5 mm, *N* = 6, and *P* = 0.5 MPa). This section conducts simulations to determine the internal gas's load capacity, stiffness, and volume flow rate for pressure equalization groove lengths *L* of 10 mm, 15 mm, 20 mm, 25 mm, and 30 mm. The influence of pressure equalization groove length on the mechanics characteristics of the throttling orifice aerostatic bearing is illustrated in Fig. 10.

Figures 10(a) and 10(c) show that varying the length of the pressure equalization groove results in minimal changes to load capacity and flow rate. Figure 10(b) illustrates that extending the pressure equalization groove's length results in a slight increase in stiffness, while having a negligible effect on the gas film thickness at the peak stiffness point. Notably, within the gas film thickness range of 10-24 μm, a groove length is 20 mm yields lower stiffness compared to other lengths.

The length of the pressure equalization groove affects the pressure distribution within the groove. However, its impact on the overall pressure distribution across the gas film is relatively minor. Consequently, altering the length of the pressure equalization groove has a negligible effect on the mechanics characteristics of throttling orifice aerostatic bearing.

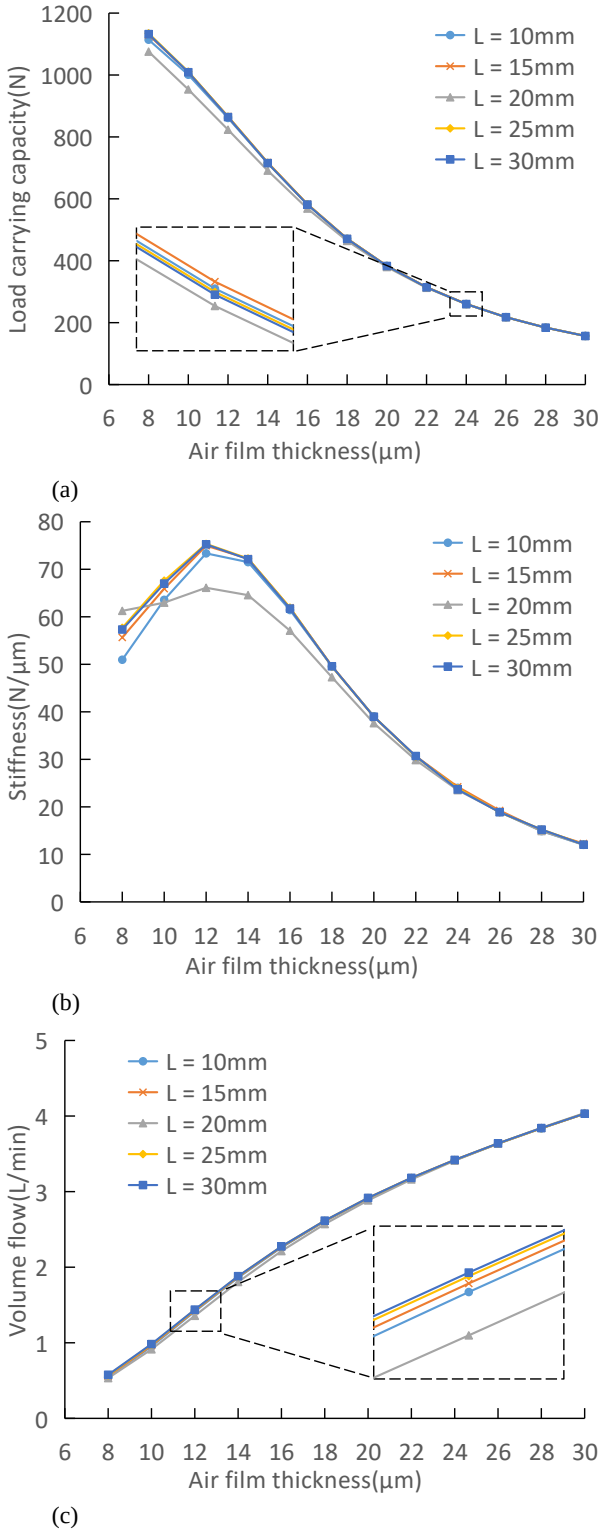

Fig. 10 Variation in load capacity, stiffness, and flow rate with different pressure-equalizing groove lengths

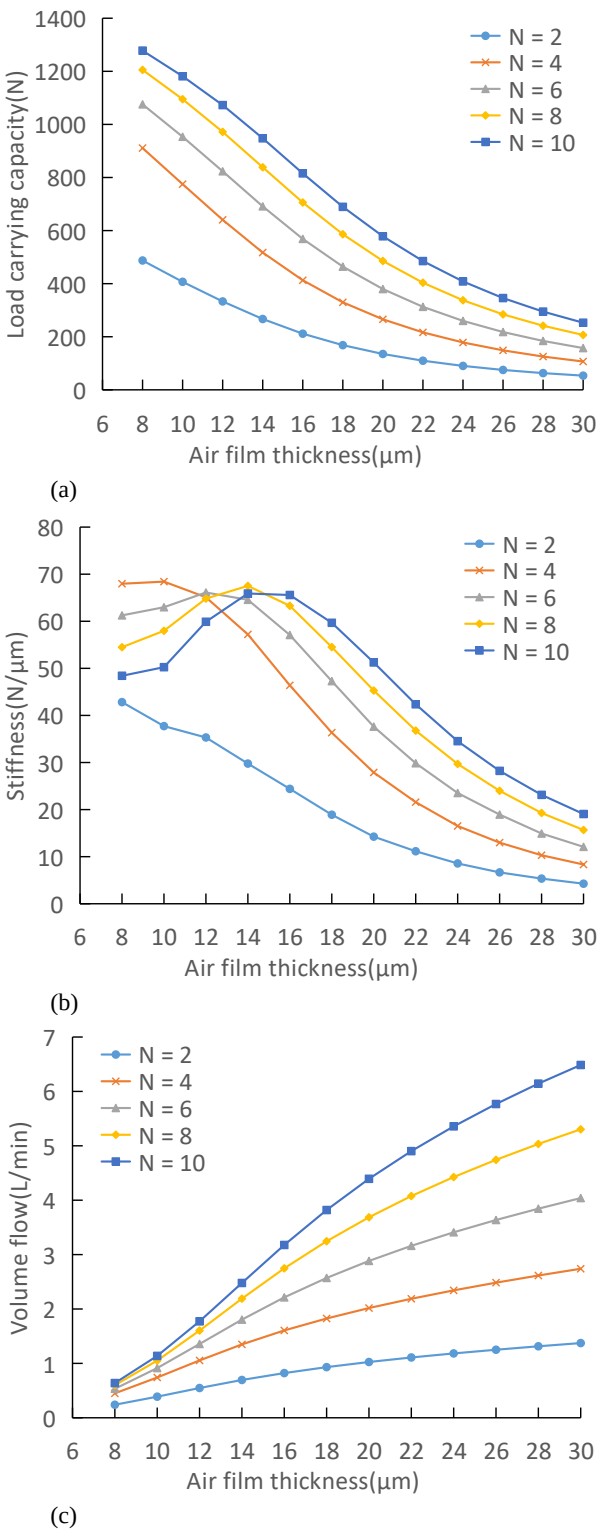

Fig. 11 Variation in load capacity, stiffness, and flow rate with different pressure-equalizing grooves numbers

3.4 Influence of Pressure Equalization Groove Quantity

This section investigates the effect of pressure equalization groove quantity on the static behavior of throttling orifice aerostatic bearing. The main structural dimensions of the aerostatic bearing remain consistent with those described earlier. At the same time, other parameters are modified (*tbb* = 0.02 mm, *wbb* = 0.5 mm, *L* = 10 mm, and *P* = 0.5 MPa). Simulations were conducted to obtain the internal gas's load capacity, stiffness, and volume flow rate for pressure equalization groove quantities *N* of 2, 4, 6, 8, and 10. Figure 11 illustrates how the number of pressure equalization grooves affects the s mechanics characteristics of aerostatic bearing with a throttling orifice.

According to Figs 11(a) and 11(c), the quantity of pressure equalization grooves significantly impacts load

capacity and flow rate. Figure 11(b) demonstrates that the stiffness for N = 2 is considerably lower within the gas film thickness range of 8-30 μm compared to other groove quantities. Reducing stiffness occurs when the number of pressure equalization grooves is increased, specifically within a gas film thickness range of 8 μm to 12 μm. However, increasing the number of grooves enhances the stiffness when the gas-film thickness surpasses 16 μm. Additionally, as the number of grooves increases, the gas film thickness at peak stiffness shifts to the right.

Increasing the number of pressure equalization grooves helps distribute the load more evenly, resulting in a more uniform pressure distribution across the gas film and reducing local deformation. Consequently, the bearing can support larger loads. However, stiffness improvement becomes less pronounced after a certain number of grooves. This observation may be attributed to factors such as saturation of the gas film pressure and restrictions on flow feature. The simulation results indicate that altering the quantity of pressure equalization grooves significantly affects the aerostatic bearing's load capacity and flow rate.

3.5 Influence of Supply Air Pressure

This section examines how supply air pressure influences the mechanics characteristics of throttling orifice aerostatic bearing that features grooves for pressure equalization. The primary structural dimensions of the aerostatic bearing remain consistent with those described earlier. At the same time, other parameters are modified (*tbb* = 0.02 mm, *wbb* = 0.5 mm, L = 10 mm, and N = 6). Simulations were conducted for supply air pressures P of 0.2 MPa, 0.3 MPa, 0.4 MPa, 0.5 MPa, and 0.6 MPa to evaluate the internal gas's load capacity, stiffness, and volume flow rate. Figure 12 illustrates how the mechanics characteristics of aerostatic bearing, which features pressure equalization grooves, is affected by the supply air pressure.

According to Figes 12(a), 12(b), and 12(c), increasing the supply air pressure significantly enhances the load capacity and stiffness while also increasing the flow rate. Load capacity and stiffness improve substantially as the supply air pressure increases; however, the gas film thickness where peak stiffness occurs remains relatively stable, i.e., around 12-14 μm. Higher supply air pressure results in greater gas velocity and flow rate through the bearing. Increased gas flow increases gas film pressure and load capacity, increasing energy consumption. Thus, there is a trade-off between performance improvement and energy consumption.

The results of the simulation demonstrate that the static performance of the throttling orifice aerostatic bearing is notably affected by the pressure equalization groove under various supply air pressures.

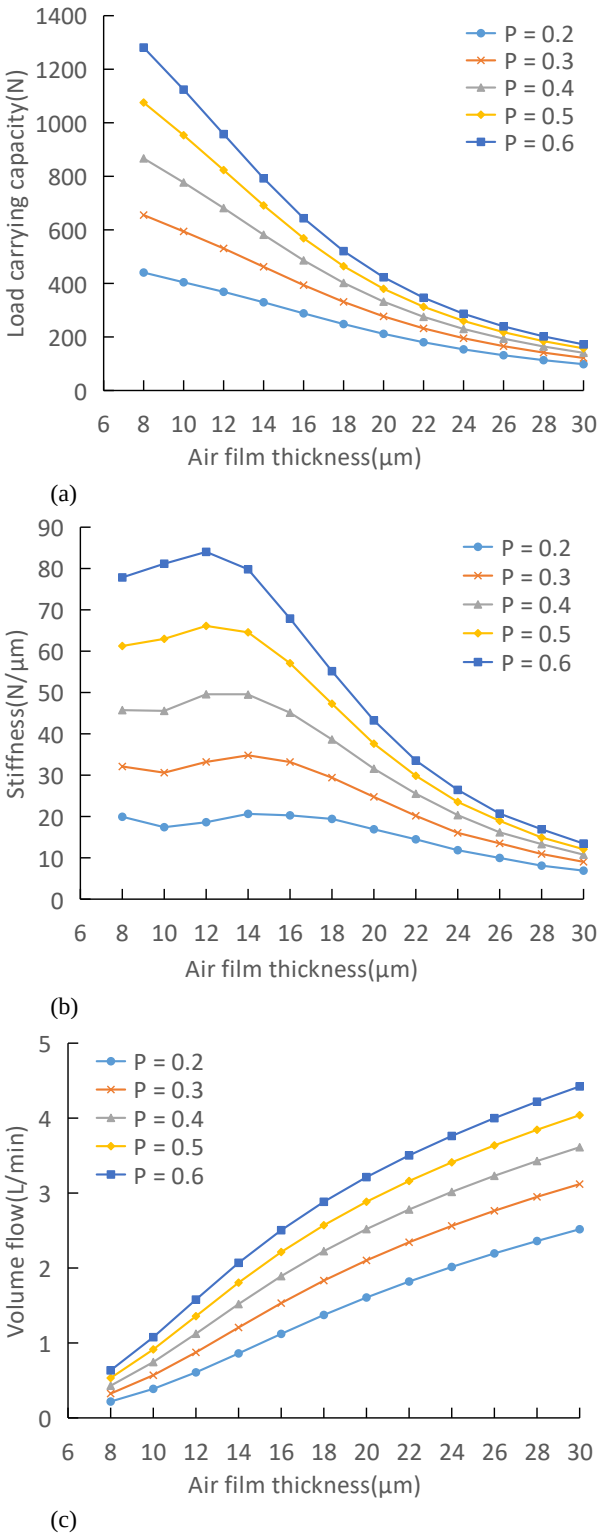

Fig. 12 Variation in load capacity, stiffness, and flow rate under different supply pressures

4. EXPERIMENTAL VALIDATION OF AEROSTATIC BEARINGS

To confirm the reliability and applicability of the numerical simulation technique using the laminar flow model for evaluating the mechanics characteristics of grooved aerostatic bearings with orifice throttling, physical prototypes were constructed, as depicted in Fig. 13. The primary parameters of the prototype are presented in Table 1, while the experimental arrangement is shown in Fig. 14. The obtained stiffness curve after conducting multiple experiments and averaging the measurement results is depicted in Fig. 15.

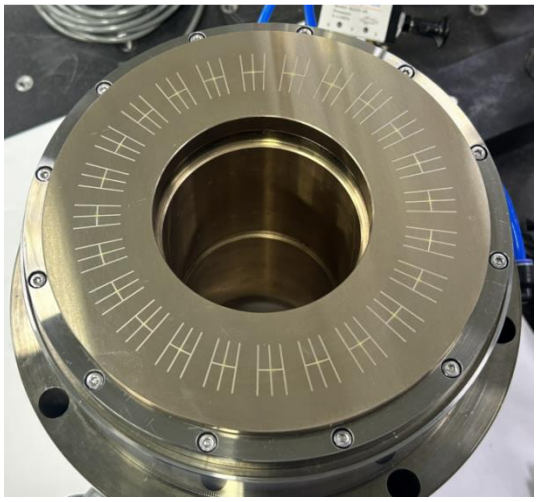

Fig. 13 Pressure-equalizing grooves orifice-restricted hydrostatic Aerostatic Bearings

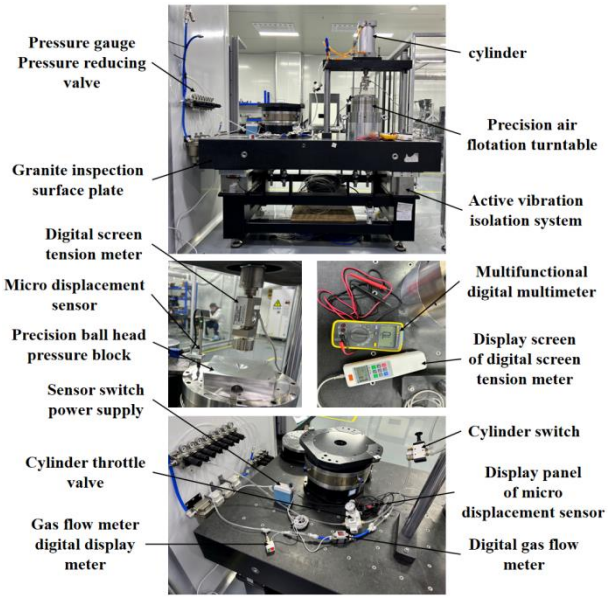

Fig. 14 Experimental measuring apparatus

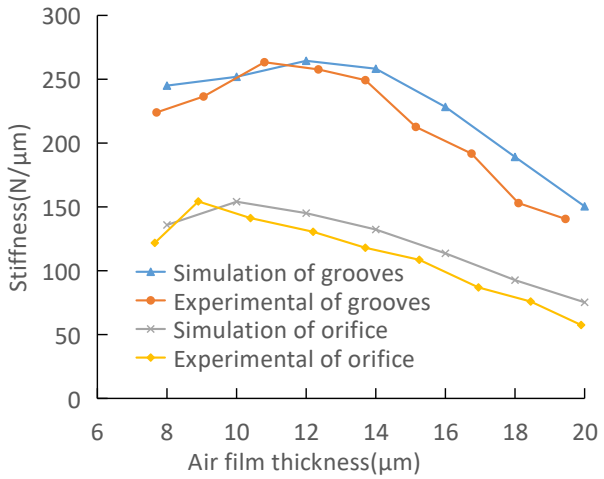

Fig. 15 Comparison between simulated and experimentally measured values

Due to inevitable errors, the finite element simulation values exceeded the experimental measurements for both bearings with and without groove structures. Additionally, the diameter of the laser-sintered orifices was slightly smaller than the ideal throttling hole diameter. Moreover, the shape of the throttling holes was approximately irregular rather than perfectly circular. Consequently, the peak position of the measured stiffness curve appeared slightly to the left of the simulated value. Despite these discrepancies, the overall agreement between theoretical and measured values is satisfactory, with the trends generally aligning. Hence, the reliability of the simulation method is validated.

The discrepancies between the finite element calculations and experimental results can be attributed to the following three reasons:

1. Machining and Manufacturing Errors: the simulation results are based on ideal conditions. However, errors inevitably arise during mechanical machining processes (e.g., inconsistent aperture sizes in laser drilling, irregular shapes of small holes, and shallow depths of grooves.). These errors significantly impact the experimental results due to the extremely small clearance of the aerostatic bearing and the high precision required for the experiment.
2. Inherent Errors in the Experimental Setup: environmental factors in the laboratory (such as temperature and humidity), measurement errors in various instruments, and precision errors inherent in the experimental equipment contribute to deviations in the final measurement values.
3. Measurement Errors: the gas-film thickness and load-bearing capacity are indirectly measured. Despite multiple measurements and averaging, some errors remain unavoidable.

5. CONCLUSIONS

A new grooved structure for the orifice throttling aerostatic bearings was designed to enhance the mechanics characteristics. Various aerostatic bearings with differing depths, widths, lengths, numbers, and supply gas pressures were explored to analyze trends in bearing load capacity, stiffness, and flow rate. The following conclusions are drawn:

(1) Enhanced performance with grooved structures. Integrating a grooved design within orifice-throttling aerostatic bearings results in a more consistent pressure distribution throughout the air film, enhancing load capacity and stiffness. However, this enhancement increases gas consumption. Compared to orifice throttling bearings without grooves, bearings with grooves exhibited a maximum load capacity increase of 81.20%, a peak stiffness increase of 71.67%, and a maximum gas flow rate increase of 53.61%.

(2) Effects of groove parameters. Increasing the depth, width, number, and supply gas pressure of the grooves led to better flow characteristics of the air film. This improvement allowed the bearing to support loads

more uniformly, increasing the bearing's load capacity and stiffness.

(3) Impact on peak stiffness. The effect of the depth and width of grooves, as well as the pressure of the supply gas, on the peak stiffness of the bearing is especially pronounced. Additionally, varying the number of grooves affects the location of the peak stiffness within the gas-film thickness. Optimizing the gas-film thickness and peak stiffness while applying a reasonable preload can enhance the bearing's load-bearing capacity, stability, and operational precision.

(4) Gas flow rate and consumption. Increasing the depth, number, and supply gas pressure of the grooves increased the velocity and flow rate of the gas passing through the bearing, increasing the gas consumption. However, groove width and length changes have a minimal impact on the flow rate.

CONFLICTS OF INTEREST

The authors declare no conflict of interest.

AUTHOR CONTRIBUTIONS

Xue Yaping: contributed to the conception of the study; **Cheng Yuanqi:** performed the experiment; **Cheng Yuanqi:** performed the data analyses and wrote the manuscript; **Lei Weining:** contributed significantly to analysis and manuscript preparation; **Gou Ning:** helped perform the analysis with constructive discussions.

REFERENCES

Belforte, G., Colombo, F., Raparelli, T., Trivella, A., & Viktorov, V. (2011). Comparison between grooved and plane aerostatic thrust bearings: static performance. *Meccanica*, *46*, 547-555. https://doi.org/10.1007/s11012-010-9307-y

Chen, D., Huo, C., Cui, X., Pan, R., Fan, J., & An, C. (2018). Investigation the gas film in micro scale induced error on the performance of the aerostatic spindle in ultra-precision machining. *Mechanical Systems and Signal Processing*, *105*, 488-501. https://doi.org/10.1016/j.ymssp.2017.10.041

Chen, G., & Chen, Y. (2021). Multi-field coupling dynamics modeling of aerostatic spindle. *Micromachines*, *12*(3), 251. https://doi.org/10.3390/mi12030251

Chen, G., Lu, Q., Ge, Y., & Zhang, W. (2022). Theoretical and experimental investigation on air film pressure field characteristics of aerostatic thrust bearing. *Proceedings of the Institution of Mechanical Engineers, Part J: Journal of Engineering Tribology*, *236*(8), 1603-1612. https://doi.org/10.1177/13506501211068942

Chen, M. F., & Lin, Y. T. (2002). Static behavior and dynamic stability analysis of grooved rectangular aerostatic thrust bearings by modified resistance network method. *Tribology International*, *35*(5), 329-338. https://doi.org/10.1016/S0301-679X(02)00012-9

Du, J., Zhang, G., & Liu, D. (2012). Influences of pressure-equalizing groove on the load capacity of externally pressurized gas journal bearings. *Journal of Mechanical Engineering*, *48*(15), 106-112. https://doi.org/10.3901/jme.2012.15.106

Gao, Q., Qi, L., Gao, S., Lu, L., Song, L., & Zhang, F. (2021). A FEM based modeling method for analyzing the static performance of aerostatic thrust bearings considering the fluid-structure interaction. *Tribology International*, *156*, 106849. https://doi.org/10.1016/j.triboint.2020.106849

Gao, S., Cheng, K., Chen, S., Ding, H., & Fu, H. (2015). CFD based investigation on influence of orifice chamber shapes for the design of aerostatic thrust bearings at ultra-high speed spindles. *Tribology International*, *92*, 211-221. https://doi.org/10.1016/j.triboint.2015.06.020

Gou, N., Cheng, K., & Huo, D. (2021). Multiscale modelling and analysis for design and development of a high-precision aerostatic bearing slideway and its digital twin. *Machines*, *9*(5), 85. https://doi.org/10.3390/machines9050085

Kodnyanko, V., Shatokhin, S., Kurzakov, A., Pikalov, Y., Strok, L., Pikalov, I., Grigorieva, O & Brungardt, M. (2021). Theoretical efficiency study of output lubricant flow rate regulating principle on the example of a two-row aerostatic journal bearing with longitudinal microgrooves and a system of external combined throttling. *Mathematics*, *9*(14), 1698. https://doi.org/10.3390/math9141698

Kumar, V., & Sharma, S. C. (2019). Effect of geometric shape of micro-grooves on the performance of textured hybrid thrust pad bearing. *Journal of the Brazilian Society of Mechanical Sciences and Engineering*, *41*, 1-24. https://doi.org/10.1007/s40430-019-2016-0

Li, T., Chen, Z., Ding, X., & Cheng, K. (2017). Design of the aerostatic linear guideway with micro-structured surfaces for ultra precision machine tools. *Journal of Mechanical Engineering*, *53*(3), 193-200. https://doi.org/10.3901/jme.2017.03.193

Liu, T., Du, J., Yao, Y., & Xie, D. (2003). Discretization and consistent conditions of lubrication equations for externally pressurized gas bearings with slot restrictors. *Journal of Mechanical Engineering*, *39*(1), 33-37. http://www.cjmenet.com.cn/CN/Y2003/V39/I1/33

Lu, Z. W., Zhang, J. A., & Liu, B. (2020). Research and analysis of the static characteristics of aerostatic bearings with a multihole integrated restrictor. *Shock and Vibration*, 1-11. https://doi.org/10.1155/2020/7426928

Otsu, Y., Somaya, K., & Yoshimoto, S. (2011). High-speed stability of a rigid rotor supported by aerostatic journal bearings with compound restrictors. *Tribology International*, *44*(1), 9-17. https://doi.org/10.1016/j.triboint.2010.09.007

Papadopoulos, C. I., Nikolakopoulos, P. G., & Kaiktsis, L. (2011). Evolutionary optimization of micro-thrust bearings with periodic partial trapezoidal surface texturing. *Journal of Engineering for Gas Turbines and Power*, *133*(1), 012301. https://doi.org/10.1115/GT2010-22495

Shang, Y., Cheng, K., Bai, Q., & Chen, S. (2022). Drag reduction analysis of the hydrostatic bearing with surface micro textures. *Applied Sciences*, *12*(21), 10831. https://doi.org/10.3390/app122110831

Sharma, S. C., Kumar, V., Jain, S. C., Sinhasan, R., & Subramanian, (1999). M. A study of slot-entry hydrostatic/hybrid journal bearing using the finite element method. *Tribology International*, *32*(4), 185-196. https://doi.org/10.1016/S0301-679X(99)00032-8

Stout, K. J., & Sweeney, F. (1984). Design of aerostatic flat pad bearings using pocketed orifice restrictors. *Tribology International*, *17*(4), 191-198. https://doi.org/10.1016/0301-679X(84)90019-7

Wang, C. C., & Lin, C. J. (2023). Dynamic analysis and machine learning prediction of a non-uniform slot air bearing system. *Journal of Computational and Nonlinear Dynamics*, *18*(1), 011007. https://doi.org/10.1115/1.4056227

Yan, R., & Zhang, H. (2021). Analysis of the dynamic characteristics of downsized aerostatic thrust bearings with different pressure equalizing grooves at high or ultra-high speed. *Advances in Mechanical Engineering*, *13*(5), 16878140211018078. https://doi.org/10.1177/16878140211018078

Yan, R., Wang, L., & Wang, S. (2019). Performance comparison between aerostatic bearings with orifice and porous restrictors based on parameter optimization. *Australian Journal of Mechanical Engineering*, *19*(4), 378-389. https://doi.org/10.1080/14484846.2019.1626529

Yoshimoto, S., Tozuka, H., & Dambara, S. (2003). Static characteristics of aerostatic porous journal bearings with a surface-restricted layer. *Proceedings of the Institution of Mechanical Engineers, Part J: Journal of Engineering Tribology*, *217*(2), 125-132. https://doi.org/10.1243/13506500360603552

Zhang, H., Guan, X., Wang, T., Robin, A. U. Z., & Mu, C. H. (2023a). Influence of pressure-equalizing groove on static load performance of aerostatic guideway. *Journal of Applied Fluid Mechanics*, *16*(5), 992-1004. https://doi.org/10.47176/jafm.16.05.1436

Zhang, G., Tang, S., Zheng, Y., He, J., Cui, H., & Liu, Y. (2023b). Numerical and experimental investigation on the performances of a liquid metal bearing with spiral groove structures. *Tribology International*, *185*, 108526. https://doi.org/10.1016/j.triboint.2023.108526

Zhang, P. (2021). Accuracy prediction model of an orifice-compensated aerostatic bearing. *Precision Engineering*, *72*, 837-846. https://doi.org/10.1016/j.precisioneng.2021.08.009

Zhao, X., Zhang, J., Dong, H., Fang, Z., & Li, J. (2017) Numerical simulation and experimental study on the gas-solid coupling of the aerostatic thrust bearing with elastic equalizing pressure groove. *Shock and Vibration*. 2017(1), 5091452. https://doi.org/10.1155/2017/5091452.

Zhao, X. L., Dong, H., Wang, Y. J., & Li, B. (2022). Study on static characteristics of annular array microporous aerostatic bearing. *Shock and Vibration*, 2022(1), 7678515. https://doi.org/10.1155/2022/7678515